

A New Speed Multiplier Coaxial Magnetic Gear

Mohd Firdaus Mohd Ab Halim^{1, 2, *}, Erwan Sulaiman¹,
Raja Nor Firdaus Kashfi Raja Othman², and Azhan Ab. Rahman^{1, 2}

Abstract—Due to certain conditions, electrical motor (EM) that operates at high speed may lead to magnetic saturation, thermal issue, and stress to rotor structure. Magnetic gear (MG) designed for speed multiplier enables the prime mover from EM to operate at lower speed while the output gear multiplies the speed by its designated gear ratio at reduced torque. In this paper, a new coaxial magnetic gear is designed for speed multiplier. The role between inner yoke with PM and pole piece is switched. The inner part of magnetic gear is made to be stationary while the pole piece becomes inner rotor. The working principle is presented analytically based on flux modulation techniques for torque and speed transmission. Torque characteristic and gear efficiency are analysed using finite element and compared with existing speed multiplier magnetic gear with the same gear ratio of 7/3. Based on the simulation result, the proposed speed multiplier MG offers 16% better torque density and 12% higher gear efficiency at higher speed range. The structure of the inner rotor is also found to be more robust as only pole piece ring together with plastic holding frame is rotated instead of yoke with PM.

1. INTRODUCTION

High speed machines are used in many applications such as compressor, machine tools, and electric vehicle. Design and control of electric motors at high-speed range have become feasible due to rapid development in converter technology. In general, classification of electrical machine (EM) is based on its output power. For the analysis purposes of this paper, high speed electrical machine can be grouped in the speed range of 10,000 rpm to 50,000 rpm. EM with speed range higher than the aforementioned is classified as a very high speed machine (VHSM). Many EM topologies can be used for high speed application which suits its respective application. For example, an induction motor with a laminated rotor is applied in a centrifugal pump; a synchronous reluctance motor is applied in a fly wheel; a permanent magnet (PM) motor is used in machine tools; and a PM synchronous reluctance motor is applied in an electric vehicle.

Several challenges need to be overcome first before EM can operate in high speed region, notably magnetic saturation, strength of the rotor, and thermal issue [1]. The strength of the rotor in a reluctance machine is considered excellent because no PM is attached to the rotating part [2, 3]. The robustness of a PM machine can also be improved by adding sleeves for surface mounted PM or by burying PM in the rotor yoke [4, 5]. Magnetic saturation in high speed and high power application is normally designed in larger size to avoid saturation. In a small sized motor, saturation can be minimized through the use of high-end core material that possesses high permeability. Integrated forced annular gap cooling method can also be deployed to manage the thermal issue in high speed operation [6]. Assuming that these challenges are tackled, EM requires a faster motor driver which will incur extra cost.

Received 1 April 2020, Accepted 10 June 2020, Scheduled 22 June 2020

* Corresponding author: Mohd Firdaus Mohd Ab Halim (mohd.firdaus@utem.edu.my).

¹ Research Center for Applied Electromagnetics, Faculty of Electrical and Electronic Engineering, Universiti Tun Hussein Onn Malaysia (UTHM) Parit Raja, Batu Pahat, Johor, Malaysia. ² Centre for Robotics & Industrial Automation, Fakulti Kejuruteraan Elektrik, Universiti Teknikal Malaysia Melaka (UTeM), Durian Tunggal, Melaka, Malaysia.

There is an alternative method that can be used to avoid the problems mentioned in a high speed EM by using additional gear. Instead of the EM operating for example at 10,000 rpm, speed multiplier multi-level mechanical gear allows the EM machine to operate at a lower speed region while the output gear multiplies the speed according to the gear ratio. Many EM applications use gear to convert torque and speed according to the gear ratio. A washing machine for instance uses a gear box to regulate speed under different operating conditions [7], while in a wind power generator, an input gear is connected to the blade shaft, and the output is connected to the speed multiplier gear to increase the generator speed [8].

Mechanical gear inherits problems such as friction loss, mechanical tooth wear and tear, as well as requiring continuous lubrication. In contrast, magnetic gear (MG) can solve the problems that appear in mechanical gear. It uses magnetic force concept of attraction and repulsion to transfer torque and rotation without any contact. The most important MG design is the coaxial magnetic gear (CMG) that uses flux modulation principle to transmit torque with high torque density [9–11]. It consists of 3 main structures; inner yoke with surface mount PM, stationary ferromagnetic pole piece, and outer yoke with surface mount PM. Based on this principle, several MG designs were developed and successfully commercialized. Even though CMG has become very well known to designers, researches are mainly focused on torque multiplier type, where gear ratio is set at > 1 [12–19]. Noticeably, there are limited publications that discuss the topic of speed multiplier where the gear ratio is set at < 1 [20–22].

In this paper, a new coaxial magnetic gear is proposed for a speed multiplier. The role between the inner yoke with PM and pole piece is switched. The inner part of magnetic gear is made stationary while the pole piece becomes the inner rotor. The working principle is presented analytically. It uses flux modulation techniques for torque and speed transmission. Torque characteristic and gear efficiency are analysed using finite element and compared with the existing speed multiplier magnetic gear with the same gear ratio of $7/3$. Based on the simulation results, the proposed speed multiplier MG offers better torque density and gear efficiency at higher speed range. The structure of the inner rotor is also recognized to be more robust as only the pole piece ring together with plastic rotates instead of yoke with PM.

2. STRUCTURE AND WORKING PRINCIPLE

Figure 1 shows the structure of a conventional PM which consists of 3 main parts: inner rotor yoke with PM, stationary alternate pole piece with plastic holding frame, and outer rotor yoke with PM. The rotational directions of the rotors are opposite to each other. Figure 2 on the other hand displays the structure of the proposed MG. The differences are that the inner rotor serves as the input rotor instead of the inner yoke with PM, and the rotational directions of rotors are the same. Table 1 indicates the dimension of the conventional design as opposed to the proposed design.

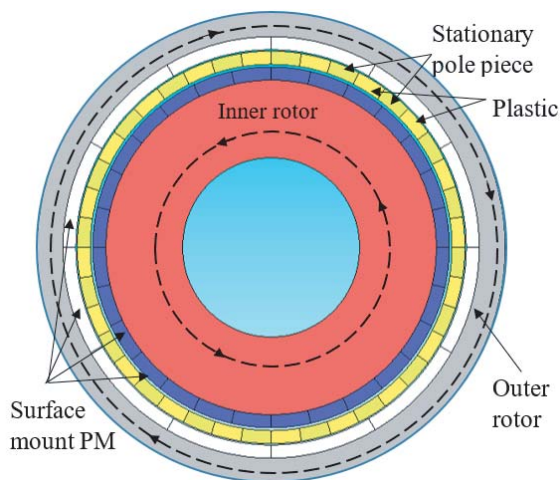


Figure 1. Structure of conventional MG.

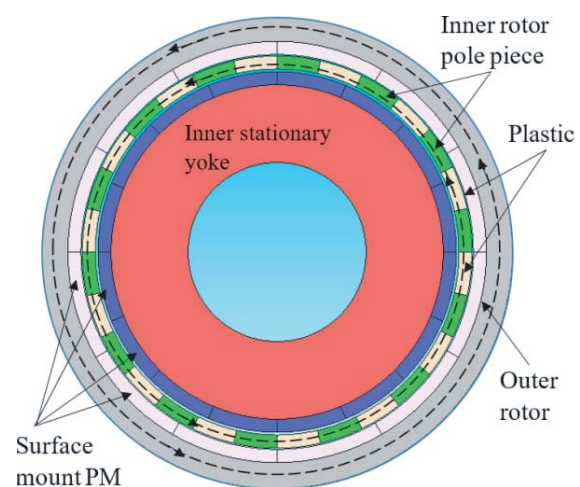


Figure 2. Structure of the proposed MG.

Table 1. Dimension of the conventional and proposed MG.

Item	Conventional MG	Proposed MG
Output	Outer PM	Pole piece
Outer pole pair	6	6
Pole piece	20	14
Inner pole pair	14	8
Gear ratio	7/3	7/3
MG radius	90 mm	90 mm
Inner pole pair radius	68.5 mm	68.5 mm
Shaft	34 mm	34 mm
Inner magnet arc	25.714°	22.5°
Pole piece arc	18°	25.714°
Outer magnet arc	30	30
Inner magnet width	5 mm	5 mm
Outer magnet width	5 mm	5 mm
Inner air gap width	1 mm	1 mm
Outer air gap width	0.5 mm	0.5 mm
Stack length	30 mm	30 mm
PM volume	1.35 × 10 ⁻⁴ m ³	

The magneto motive force (mmf) at the inner and outer air gaps can be expressed in simplified Equations (1) and (2), respectively [23, 24], assuming a sinusoidal behaviour

$$F_i(\theta) = F_{mi}\cos(p_i(\theta - w_it)) \tag{1}$$

$$F_o(\theta) = F_{mo}\cos(p_o(\theta - w_ot)) \tag{2}$$

where $F_i(\theta)$, $F_o(\theta)$, F_{mi} , F_{mo} , p_i , p_o , w_it , w_ot are the mmf of the inner and outer air gaps, amplitude of the mmf, pole pair and offset angle of one of the inner pole pairs at inner and outer air gaps.

The fixed permeance and varying permeance of the overall MG is

$$P_r = P_{avg} + P_p\cos(n_p(\theta - w_pt)) \tag{3}$$

where P_r , P_{avg} , P_p , n_p , and w_pt are the permeance of the MG, average permeance at the yoke, magnet and pole piece, permeance amplitude, number of pole pieces, and offset angle to one of the pole piece segment, respectively. The air-gap flux distribution can be expressed as

$$\emptyset_i(\theta) = F_i(\theta) P_r \tag{4}$$

$$\emptyset_o(\theta) = F_o(\theta) P_r \tag{5}$$

The flux acting on the pole piece is the summation of flux in inner air gap and outer air gap, expressed as

$$\emptyset_{pp}(\theta) = \emptyset_i(\theta) + \emptyset_o(\theta) \tag{6}$$

where $\emptyset_i(\theta)$ and $\emptyset_o(\theta)$ is the air gap flux at the inner and outer sides of the pole piece. The trigonometric [25] to solve the multiplication above is

$$\cos(X) \times \cos(Y) = \frac{1}{2} \cos(X - Y) + \cos(X + Y) \tag{7}$$

Thus, Equations (4) and (5) are written as

$$\left. \begin{aligned} \emptyset_k(\theta) &= F_{mk}P_{avg} \cos(p_k(\theta - w_kt)) \\ &+ \frac{F_{ms}P_p}{2} \cos((n_p - p_k)\theta + p_kw_kt - n_pw_pt) \\ &+ \frac{F_{ms}P_p}{2} \cos((n_p + p_k)\theta - p_kw_kt - n_pw_pt) \end{aligned} \right\} \tag{8}$$

where k represents the air gap location either in inner or outer area. Equation (8) consists of 3 components, where the first component is the fundamental flux expression, and the second and third components are the modulated harmonics 1 and 2. To determine the pole pair for any given gear ratio, the magnetic field density and its Discrete Fourier transform with only inner rotor and pole piece are simulated in static analysis shown in Figure 3(a) and Figure 3(b) for conventional MG and Figure 4(a) and Figure 4(b) for the proposed MG.

In Figure 3(b), the highest harmonic component of the conventional model occurs at the 14th period which is equivalent to the inner pole pairs. The 2nd harmonic occurs at the 6th period which reveals the number of the outer pole pairs. In order to transfer the inner-torque to the outer air gap, the number of pole pairs must be created equal to the n th harmonic which has the highest magnitude, for this case, 6th. The 3rd harmonic component is not selected to be the pole pair because it generates less magnitude. These harmonic components agree with Equation (6) where the first row of the equation represents the fundamental component; the second row of the equation represents harmonic component 1; and the third row of the equation represents harmonic component 2. In Figure 4(b), the highest harmonic component of the proposed model occurs at the 8th period which is equivalent to the inner pole pair. The 2nd harmonic occurs at the 6th period which reveals the number of outer pole pairs. Taking these as a general rule, the pole pair relation can be expressed as

$$p_i + p_o = n_p \quad (9)$$

where p_i and p_o are the inner pole pair and outer pole pair, respectively, and n_p is the number of pole

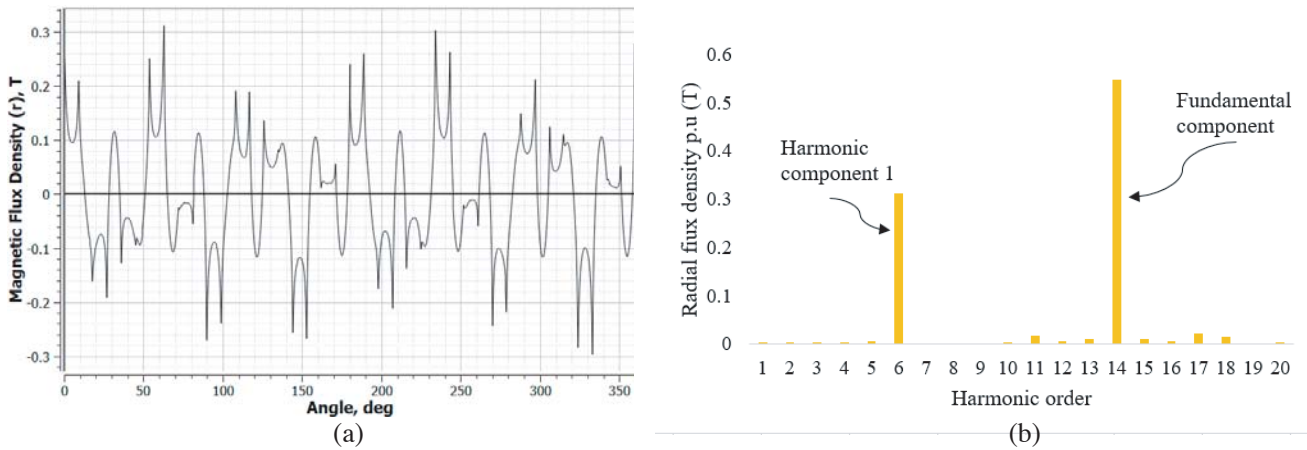


Figure 3. Conventional model. (a) Radial flux density. (b) DFT harmonic order.

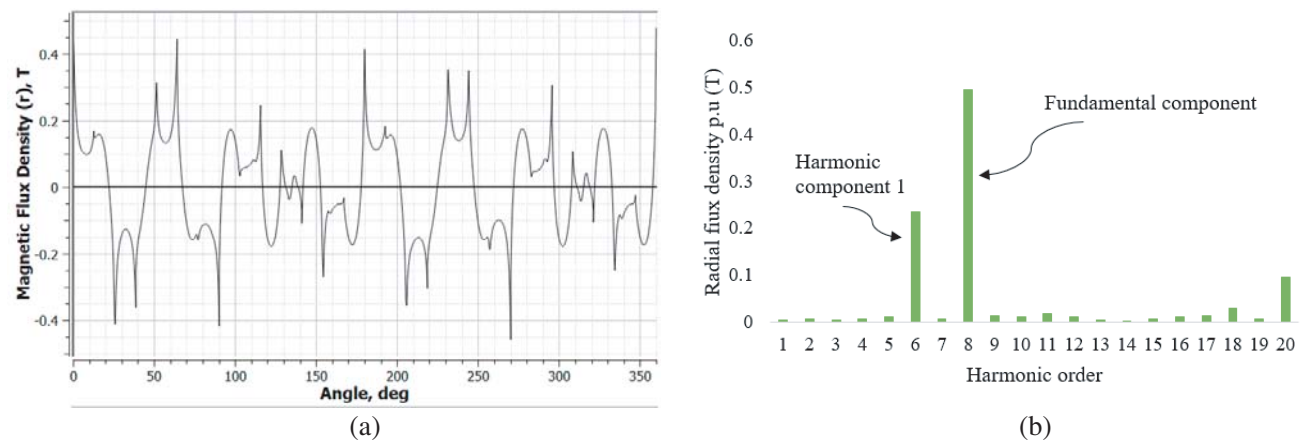


Figure 4. Proposed model. (a) Radial flux density. (b) DFT harmonic order.

pieces. If each term in Eq. (8) is multiplied by its respective rotational velocity of the space harmonic, the equation becomes

$$w_i p_i + w_o p_o = w_p n_p \quad (10)$$

where w_o is the speed of outer rotor. The terms represent the vital parts of a flux modulation magnetic gear. If a pole piece is let to be stationary such that in conventional magnetic gear, $w_p n_p$ term will become zero. Then, the gear ratio G_r can be written as;

$$G_r = \frac{w_i}{w_o} = -\frac{p_o}{p_i} \quad (11)$$

For conventional model, substituting $p_i = 14$ and $p_o = 6$, the gear ratio G_r becomes $-3/7$. The negative sign indicates that the rotation directions of the rotors are opposing each other.

For the proposed model, when the inner pole pair with surface mount PM is let to be stationary, the gear ratio can be written as

$$G_r = \frac{w_p}{w_o} = \frac{p_o}{n_p} \quad (12)$$

Substituting $p_o = 6$ and $n_p = 14$, the gear ratio G_r becomes $3/7$. The positive gear ratio indicates that both rotors rotate in the same direction. In Equation (11), the output of the conventional model is represented by the outer pole pair while in Equation (12), the output of proposed model is represented by the pole piece. Both models yield fractional gear ratio of $|3/7|$ which is equivalent to speed ratio of 3:7 (input to output).

The electromagnetic (EMT) torque acting on the inner air gap can be written as Eq. (13) using Maxwell stress tensor [26–28]

$$T_i = \frac{l r_i^2}{\mu_o} \int_{\theta=0}^{2\pi} B_{r_i}(r_i, \theta) \times B_{\theta_i}(r_i, \theta) \cdot d\theta \quad (13)$$

where T_i is the EM torque acting on the inner air gap, l the axial length of MG, r_i the radius taken as the integration path along the circumference of the air gap, B_{r_i} the integral average of the radial component of flux density distribution at radius r_i , B_{θ_i} the integral average of the tangential flux density distribution at radius r_i , and ϑ the angle of the inner air gap. The EMT torque acting on the outer air gap can be written as,

$$T_o = \frac{l r_o^2}{\mu_o} \int_{\theta=0}^{2\pi} B_{r_o}(r_o, \theta) \times B_{\theta_o}(r_o, \theta) \cdot d\theta \quad (14)$$

where T_o is the EMT torque acting on the outer air gap, r_o the radius taken as the integration path along the circumference of the air gap, B_{r_o} the integral average of the radial component of the flux density distribution at radius r_o , B_{θ_o} the integral average of the tangential flux density distribution at radius r_o , and ϑ the angle of the outer air gap. The torque required by the external force to rotate the inner rotor is the same as Eq. (14). The torque produced in the pole piece is the summation of the EMT torques acting in the inner air gap and outer air gap which can be written as:

$$T_{pp} = \frac{l}{\mu_o} \int_{\theta=0}^{2\pi} r_i \{B_{r_i}(r_i, \theta_i) \times B_{\theta_i}(r_i, \theta_i)\} + r_o \{B_{r_o}(r_o, \theta_o) \times B_{\theta_o}(r_o, \theta_o) \cdot d\theta\} \quad (15)$$

where T_{pp} is the torque acting on the pole piece when either inner pole pair or outer pole pair is stationary. This equation can be used when the radial and tangential component of the flux density is known.

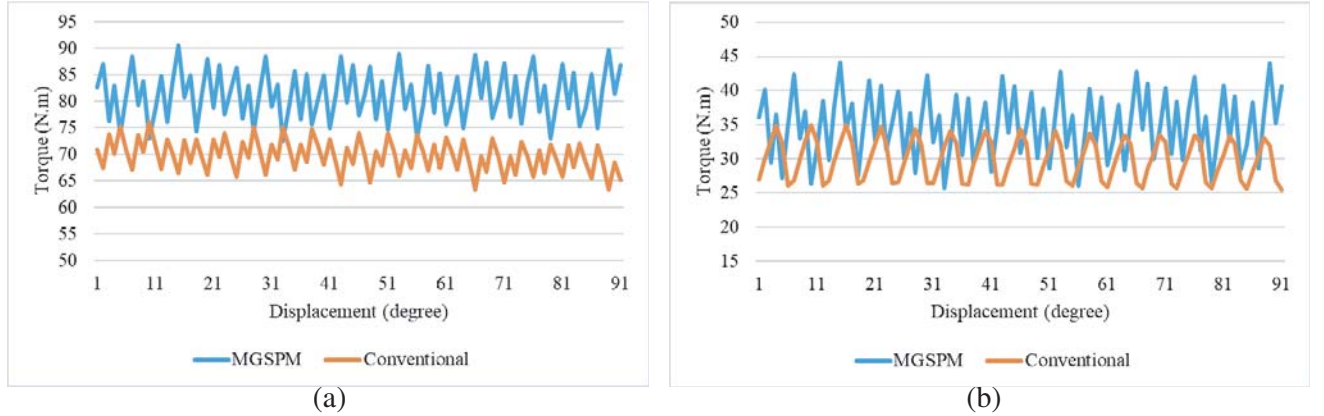
3. FINITE ELEMENT SIMULATION

3.1. Torque Analysis

The torque performances of the proposed MG are evaluated by finite-element analysis software JMAG Designer version 16. These data are compared against the conventional model. Material selection in Table 2 used in the simulation is based on several similar publications [29–34]. The rotational speed setting for conventional model is 300 rpm for inner pole pair rotor and 700 rpm for outer pole pair

Table 2. Material selection in torque analysis.

Component	Material	Remarks
Inner yoke		
Outer yoke	NSSMC 35H210	Resistivity of $5.9 \times 10^{-7} \Omega$
Pole piece		
Magnet	Hitachi NEOMAX 35AH	1.2 T residual
Plastic holder	Plastic	Placed between pole piece

**Figure 5.** Torque waveform in conventional and proposed MG. (a) Input rotor torque. (b) Output rotor torque.

rotor, while the pole piece is let stationary. The transient analysis is set for 1/4 full rotation. No eddy current is allowed for this analysis. Figure 5 shows the torque waveform for conventional model and the proposed model at (a) input rotor and (b) output rotor.

The proposed MG produces higher input and output torque than conventional model. The torque waveform also shows torque ripple in both models especially in the proposed MG. Torque ripple can be calculated as follows

$$T_r = \frac{T_{\max} - T_{\min}}{T_{\text{avg}}} \quad (16)$$

where T_r is the torque ripple, T_{\max} the maximum value of the torque, T_{\min} the minimum value of the torque, and T_{avg} the average torque. Torque density can be calculated as

$$T_d = \frac{2 \int_0^{\frac{\pi}{2}} T_o(\theta) d(\theta)}{\pi V_{ol}} \quad (17)$$

where T_d is the torque density, $T_o(\theta)$ the output rotor torque function in mechanical degree, and V_{ol} the active volume of the MG including air gap. Table 3 summarizes the simulation results for this analysis. The output torques for both models are smaller than the input torque because of < 1 gear ratio. Even though the torque performance in the proposed MG is better than conventional model, the torque ripple in the proposed MG is 20% higher than the conventional model. In switched reluctance motor (SRM), torque ripple is also higher than that in PM motor [35]. Unfortunately, unlike SRM, MG has no armature coil to minimize the torque ripple.

Table 3. Torque analysis simulation result summary.

Torque analysis	Proposed	Conventional
Input torque	81.31	69.77
Output torque	34.86	29.94
Input torque ripple	22.17	18.31
Output torque ripple	52.54	32.01
Torque density	58.05	49.87
Torque to PM ratio	257.74	221.40

3.2. Gear Efficiency

In this analysis, the integral average of the torque is calculated as

$$\tau = \frac{4}{T} \int_0^{T/4} \tau(t) dt \tag{18}$$

where τ is the integral average of the torque, $\tau(t)$ the function of torque in time, and T the period of full rotation. The integral interval is between time 0 and $T/4$. The efficiency of the MG is expressed as follows:

$$\eta_G = \frac{\tau_o v_o}{\tau_i v_i} \tag{19}$$

where τ_o is the integral average of the output rotor torque, v_o the output rotor speed, τ_i the integral average of the input torque, and v_i the speed of the input rotor. The speed pair selected for this simulation are shown in Table 4.

Table 4. Speed selection for gear efficiency study.

	Speed (rpm)	
	Input rotor	Output rotor
Case 1	900	2100
Case 2	2100	4900
Case 3	5400	12600
Case 4	8100	18900
Case 5	10800	25200

The generation of eddy current in the PM is due to the variation in magnetic flux density at the air gap. MG uses a high power density rare-earth PM to produce better torque density. Hence, its eddy current magnitude is much higher when rare earth with high flux density is utilized. As the speed of the rotor increases, the variation of magnetic field becomes larger and directly increases joule loss of MG [36, 37]. Figure 7 shows the gear efficiency degradation in the proposed and conventional models in 5 cases. In cases 1 and 2, gear efficiency of the conventional model is slightly higher than proposed MG. In case 3 onwards, the gear efficiency for the proposed MG degrades less than the conventional model and produces better efficiency as shown in the linear trend line in Figure 6. Figure 7 shows the distribution of Joule loss between inner PM and outer PM for (a) proposed model and (b) conventional model. The magnitude of the Joule loss does not reflect the gear efficiency trend line because the prime mover power required in conventional model is only 22% of the proposed MG. Table 5 summarizes the result for gear efficiency analysis. Even though gear efficiency in the proposed MG registers better values, the torque ripple produced in this model is double of the conventional model at the output rotor.

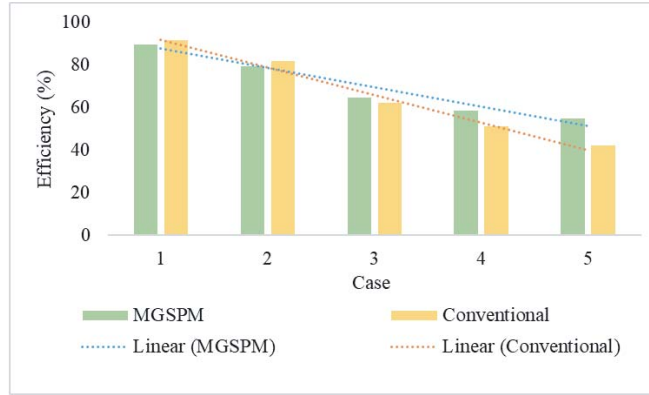


Figure 6. Gear efficiency of proposed model and conventional model.

Table 5. Summary of gear efficiency analysis.

Model	Cases	Torque (N.m)		Torque ripple (%)		Efficiency (%)
		Input	Output	Input	Output	
Proposed	1	81.55	38.97	21.94	46.67	89.69
	2	82.14	44.21	21.22	39.91	79.62
	3	83.38	55.18	20.09	52.07	64.76
	4	84.29	61.63	20.41	59.44	58.61
	5	84.97	66.41	21.42	65.40	54.83
Conventional	1	71.38	28.02	15.84	24.05	91.60
	2	73.29	25.77	15.00	21.75	82.05
	3	77.91	20.85	16.49	19.35	62.44
	4	80.84	17.76	20.20	23.07	51.25
	5	83.34	15.15	23.49	25.94	42.42

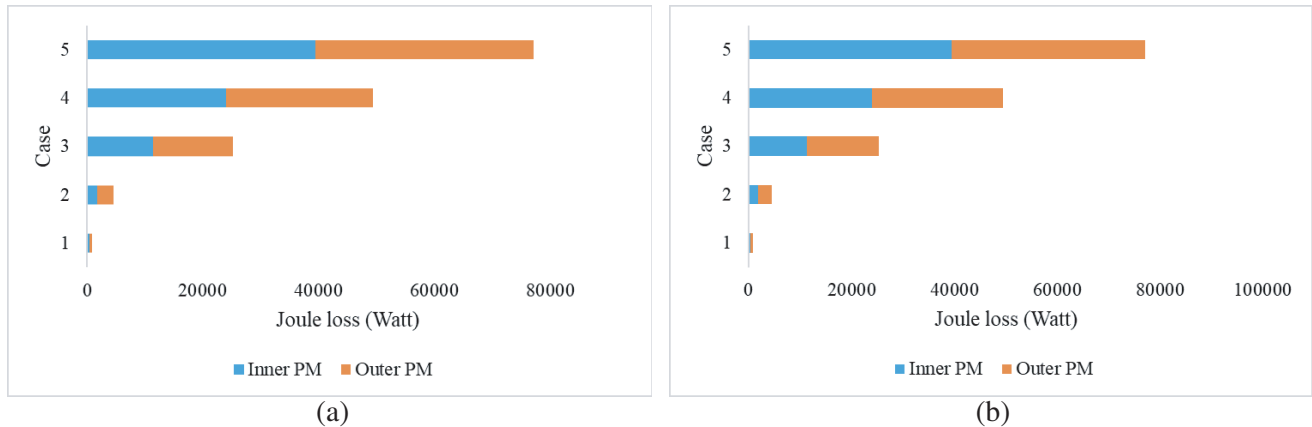


Figure 7. Joule loss at inner PM and outer PM. (a) Proposed model. (b) Conventional mode.

4. CONCLUSION

In this paper, a new speed multiplier coaxial magnetic gear is proposed. Unlike the conventional MG, the new design swaps the input rotor from the surface mount PM with yoke to the pole piece. This change minimizes the stress exerted on the initial setup where the PM with yoke is moving. The operation of

the proposed MG has been discussed analytically. The torque, torque density, torque ripple, and gear efficiency are simulated using finite element software with and without Joule loss inclusion. The results of the simulations are compared against the conventional model with the same size and gear ratio. Based on the simulation results, the torque density of the proposed MG reflects $\sim 16\%$ better torque density than the conventional model. Similarly, the gear efficiency of the proposed MG indicates 12% better efficiency than the conventional model at higher speed pair of 10,800 rpm : 25,200 rpm. This result shows its applicability to operate in high speed region besides having better rotor strength. However, the improvement comes with drawbacks in torque ripple. The highest torque ripple in conventional model is 25% whereas in the proposed model it is found to be 65%. This drawback is expected for a machine that rotates based on reluctance torque. Future works will be carried out to focus on minimizing the torque ripple and evaluating the mechanical strength of CMG. In conclusion, this proposed CMG can increase EM speed and act as an alternative to the mechanical gear and conventional MG.

ACKNOWLEDGMENT

Many thanks to the Universiti Tun Hussein Onn Malaysia (UTHM) and Universiti Teknikal Malaysia Melaka (UTeM). This work was supported by the Research Management Centre, UTHM. [Research Fund E15501].

REFERENCES

1. Atay, F. M., "Magnetic saturation and steady-state analysis of electrical motors," *Appl. Math. Model.*, Vol. 24, No. 11, 827–842, 2000.
2. Ahn, J.-W. and G. F. L. Lukman, "Switched reluctance motor: Research trends and overview," *China Electrotech. Soc. Trans. Electr. Mach. Syst.*, Vol. 2, No. 4, 339–347, 2019.
3. Ion, B. and T. Lucian, *Reluctance Electric Machines: Design and Control*, 2018.
4. Chen, L. L., C. S. Zhu, Z. Zhong, B. Liu, and A. Wan, "Rotor strength analysis for high-speed segmented surface-mounted permanent magnet synchronous machines," *IET Electr. Power Appl.*, Vol. 12, No. 7, 979–990, 2018.
5. Dong, J., Y. Huang, L. Jin, and H. Lin, "Comparative study of surface-mounted and interior permanent-magnet motors for high-speed applications," *IEEE Trans. Appl. Supercond.*, Vol. 26, No. 4, 26–29, 2016.
6. Tüysüz, A., F. Meyer, M. Steichen, C. Zwyssig, and J. W. Kolar, "Advanced cooling methods for high-speed electrical machines," *IEEE Trans. Ind. Appl.*, Vol. 53, No. 3, 2077–2087, 2017.
7. Karim, N., "How washing machines work," 2000, <https://www.howstuffworks.com>.
8. Lombardo, T., "Shifting gears on wind turbines," 2013, <https://www.engineering.com>.
9. Atallah, K. and D. Howe, "A novel high-performance linear magnetic gear," *IEEE Trans. Magn.*, Vol. 37, No. 4, 2844–2846, 2001.
10. Atallah, K., S. D. Calverley, and D. Howe, "Design, analysis and realisation of a high-performance magnetic gear," *IEE Proceedings — Electric Power Appl.*, Vol. 150, No. 2, 139–145, 2004.
11. Atallah, K., S. D. Calverley, and D. Howe, "High-performance magnetic gears," *J. Magn. Magn. Mater.*, Vol. 272–276, No. SUPPL. 1, 1727–1729, 2004.
12. Tallerico, T. F., J. J. Scheidler, and Z. A. Cameron, "Electromagnetic mass and efficiency of magnetic gears for electrified aircraft," *2019 AIAA/IEEE Electr. Aircr. Technol. Symp.*, 1–25, August 2019.
13. Kawanishi, K., K. Matsuo, T. Mizuno, K. Yamada, T. Okitsu, and K. Matsuse, "Development and performance of high-speed SPM synchronous machine," *2018 Int. Power Electron. Conf. IPEC-Niigata — ECCE Asia 2018*, 169–176, 2018.
14. Gouda, E., S. Mezani, L. Baghli, and A. Rezzoug, "Comparative study between mechanical and magnetic planetary gears," *IEEE Trans. Magn.*, Vol. 47, No. 2, 439–450, 2011.
15. Huang, C. C., M. C. Tsai, D. G. Dorrell, and B. J. Lin, "Development of a magnetic planetary gearbox," *IEEE Trans. Magn.*, Vol. 44, No. 3, 403–412, 2008.

16. Gim, C. S., E. J. Park, S. Y. Jung, and Y. J. Kim, "Torque characteristic analysis of coaxial magnetic gear according to fillet parameter of pole piece," *ICEMS 2018 — 2018 21st Int. Conf. Electr. Mach. Syst.*, No. 1, 2557–2560, 2018.
17. Wang, L. L., J. X. Shen, Y. Wang, and K. Wang, "A novel magnetic-g geared outer-rotor permanent-magnet brushless motor," *Proceedings of the 4th IET International Conference on Power Electronics and Drives 2008*, 33–36, 2008.
18. Jian, L., K. T. Chau, and J. Z. Jiang, "A magnetic-g geared outer-rotor permanent-magnet brushless machine for wind power generation," *IEEE Trans. Ind. Appl.*, Vol. 45, No. 3, 954–962, 2009.
19. Sun, L., M. Cheng, and H. Jia, "Analysis of a novel magnetic-g geared dual-rotor motor with complementary structure," *IEEE Trans. Ind. Electron.*, Vol. 62, No. 11, 6737–6747, 2015.
20. Pop, C. V. and D. Fodorean, "In-wheel motor with integrated magnetic gear for extended speed applications," *2016 Int. Symp. Power Electron. Electr. Drives, Autom. Motion*, Vol. 1143, 413–418, 2016.
21. Molokanov, O., P. Dergachev, S. Osipkin, E. Kuznetsova, and P. Kurbatov, "A novel double-rotor planetary magnetic gear," *IEEE Trans. Magn.*, Vol. 54, No. 11, 1–5, 2018.
22. Park, E. J., C. S. Kim, S. Y. Jung, and Y. J. Kim, "Dual magnetic gear for improved power density in high-gear-ratio applications," *ICEMS 2018 — 2018 21st Int. Conf. Electr. Mach. Syst.*, 2529–2532, 2018.
23. Gerber, S., "Evaluation and design aspects of magnetic gears and magnetically geared electrical machines," Stellenbosch University, 2015.
24. Neves, C. G. C. and A. F. F. Filho, "Magnetic gearing electromagnetic concepts," *J. Microwaves, Optoelectron. Electromagn. Appl.*, Vol. 16, No. 1, 108–119, 2017.
25. Joyce, D. E., "Summary of trigonometric identities," 2020.
26. Neves, C. G. C., D. L. Figueiredo, and A. S. Nunes, "Magnetic gear: A review," *2014 11th IEEE/IAS Int. Conf. Ind. Appl.*, 1–6, 2014.
27. Lubin, T., S. Mezani, and A. Rezzoug, "Analytical computation of the magnetic field distribution in a magnetic gear," *IEEE Trans. Magn.*, Vol. 46, No. 7, 2611–2621, 2010.
28. Zhang, X., X. Liu, C. Wang, and Z. Chen, "Analysis and design optimization of a coaxial surface-mounted permanent-magnet magnetic gear," *Energies*, Vol. 7, 8535–8553, 2014.
29. Ye, X., "Kilowatt three-phase rotary transformer design for permanent magnet DC motor with on-rotor drive system," MID Sweden University, 2016.
30. Tzanakis, I., M. Hodnett, I. V. Bogdanov, S. S. Kozub, K. Sugo, and S. B. Kim, "Fundamental study on the magnetic field control method using multiple HTS coils for Magnetic Drug Delivery System Fundamental study on the magnetic field control method using multiple HTS coils for Magnetic Drug Delivery System," *Journal of Physics: Conference Series*, 1–6, 2017.
31. I, E. M., E. Sulaiman, and A. Zarafi, "A high torque segmented outer rotor permanent magnet flux switching motor for motorcycle propulsion," *MUCET 2017*, Vol. 150, 1–6, 2018.
32. Ridge, A. N., S. Ademi, R. A. McMahon, and H. Kelly, "Ferrite-based axial flux permanent magnet generator for wind turbines," *J. Eng.*, Vol. 2019, No. PEMD 2018, 3942–3946, 2019.
33. Kimiabeigi, M., J. D. Widmer, R. S. Sheridan, A. Walton, and R. Harris, "Design of high performance traction motors using cheaper grade of materials," *8th IET International Conference on Power Electronics, Machines and Drives (PEMD 2016)*, Vol. 1, 1–7, 2016.
34. Kouhshahi, M. B., V. M. Acharya, M. Calvin, and J. Z. Bird, "Designing and experimentally testing a flux-focusing axial flux magnetic gear for an ocean generator application," *IET Electr. Power Appl.*, Vol. 13, No. 8, 1212–1218, 2019.
35. Cai, H., H. Wang, M. Li, S. Shen, Y. Feng, and J. Zheng, "Torque ripple reduction for switched reluctance motor with optimized PWM control strategy," *Energies*, Vol. 11, No. 11, 2018.
36. Mateev, V. and I. Marinova, "Loss estimation of magnetic gears," *Electr. Eng.*, No. 0123456789, 1–13, 2019.
37. Filippini, M., et al., "Magnetic loss analysis in coaxial magnetic gears," *Electron.*, Vol. 8, No. 11, 1–15, 2019.